ChemComm

COMMUNICATION

View Article Online
View Journal | View Issue

Cite this: *Chem. Commun.*, 2025, **61**, 16568

Received 7th August 2025,
Accepted 11th September 2025

DOI: 10.1039/d5cc04517g

rsc.li/chemcomm

Interfacial electric field in Zr-MOF-grafted carbon nitride to boost H_2O_2 piezo-synthesis under ambient conditions

Jingyi Yang,[a] Zhi Li,*[ac] Huiru Chen,[a] Jie Leng,[a] Li Gong*[b] and Mingshan Zhu*[ac]

Harnessing interfacial electric fields offers a promising route to boost piezocatalytic efficiency. Here, we grafted Zr-MOF onto carbon nitride to construct an interfacial electric field, leading to a hydrogen peroxide production rate of 4.76 mmol g^{-1} h^{-1} *via* water oxidation and the oxygen reduction reaction.

Hydrogen peroxide (H_2O_2) has emerged as a versatile and environmentally benign oxidant with wide-ranging applications in energy storage, water treatment, and green synthesis.[1] Traditional H_2O_2 production relies on the energy-intensive anthraquinone process, which suffers from high carbon emissions and complex infrastructure.[2] The direct synthesis of H_2O_2 from oxygen and water offers a sustainable alternative, but conventional thermostatic approaches often require noble metal catalysts and hazardous conditions.[3] In this context, piezocatalysis, an emerging technology that converts mechanical energy into chemical energy, holds great promise for sustainable H_2O_2 production.[4,5] Its mechanism relies on stress-induced charge separation within piezoelectric materials, which initiates redox reactions between O_2 and H_2O to generate H_2O_2. However, electrons and holes produced under piezoelectric excitation rapidly recombine, limiting the catalytic efficiency.[6] Therefore, promoting effective charge separation remains a key challenge for advancing piezocatalytic systems.[7–9]

To overcome such rapid recombination of charge carriers, previous works have mainly focused on strategies such as elemental doping[10] and introducing defect sites[11] to improve charge-carrier–separation efficiency.[12] In recent years, constructing an internal electric field (IEF) has been recognized as an effective method for improving the reactivity and selectivity of catalytic reactions in the energy and environmental fields.[13] Zhang *et al.* prepared a step-scheme heterojunction ZnO/COF(TpPa-Cl) using a simple electrostatic self-assembly method and studied its photocatalytic H_2O_2 generation performance.[14] However, research on using the IEF for enhancing charge carrier separation in piezocatalysis remains relatively scarce.

Carbon nitride (C_3N_4) was first reported in 2019 to have piezoelectrically catalyzed hydrogen-peroxide-producing activity, attributed to its excellent piezoelectric properties.[15–17] However, the poor charge-carrier–separation ability of pure C_3N_4 limits the efficiency of its piezoelectric-catalyzed synthesis of H_2O_2, which may be due to its fast carrier complexation.[18–21] To address this critical issue, we constructed the IEF to efficiently promote piezoelectric carrier separation by grafting MOFs[22,23] onto the carbon nitride surface taking advantage of their tunable electronic structures and catalytic sites.[24,25]

We integrated C_3N_4 with UiO-66 through electrostatic self-assembly to create a composite exhibiting enhanced interfacial charge modulation. The optimized C_3N_4/UiO-66 system demonstrated exceptional piezocatalytic performance, achieving an H_2O_2 production rate of 4.76 mmol g^{-1} h^{-1} under ambient conditions, representing 12.1-fold and 11.5-fold improvements over pristine C_3N_4 and UiO-66, respectively. Electron paramagnetic resonance (EPR) spectra showed the simultaneous presence of $^*O_2^-$ and $^\bullet$OH radical species, indicating the cooperative use of oxygen reduction (ORR) and water oxidation (WOR) pathways. The IEF intensity of the C_3N_4/MOF was assessed by taking zeta potential measurements, and performing open-circuit voltage tests, and was found to be 1.17 times higher than that of pristine C_3N_4. This work has provided a generalizable strategy for developing advanced piezocatalytic WOR materials.

C_3N_4/UiO-66 composites were prepared *via* electrostatic self-assembly.[14] Transmission electron microscopy (TEM) showed that UiO-66 indeed grafted onto the C_3N_4 surface (Fig. S1–S3) and XRD analysis revealed a shift in the (002) diffraction peak

[a] *Guangdong Engineering Technology Research Center of Water Treatment Processes and Materials, College of Environment and Climate, Jinan University, Guangzhou 511443, China. E-mail: zhili@jnu.edu.cn, zhumingshan@jnu.edu.cn*

[b] *Instrumental Analysis and Research Center, Sun Yat-Sen University, Guangzhou, 510275, China. E-mail: gongli2@mail.sysu.edu.cn*

[c] *Guangdong Provincial Key Laboratory of Spine and Spinal Cord Reconstruction, The Fifth Affiliated Hospital of Jinan University (Heyuan Shenhe People's Hospital), Heyuan 517465, China*

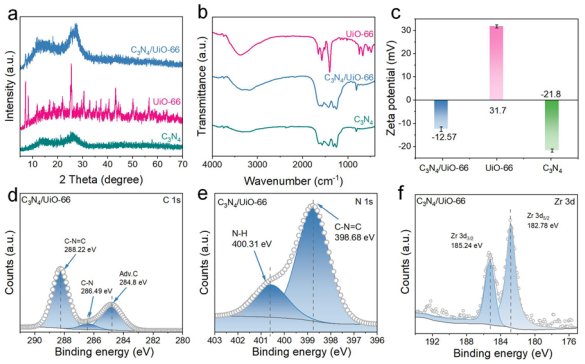

Fig. 1 (a) XRD patterns, (b) FT-IR spectra, and (c) zeta potential values of C_3N_4/UiO-66, UiO-66 and C_3N_4. (d) C 1s, (e) N 1s, and (f) Zr 3d regions of the XPS spectrum of C_3N_4/UiO-66.

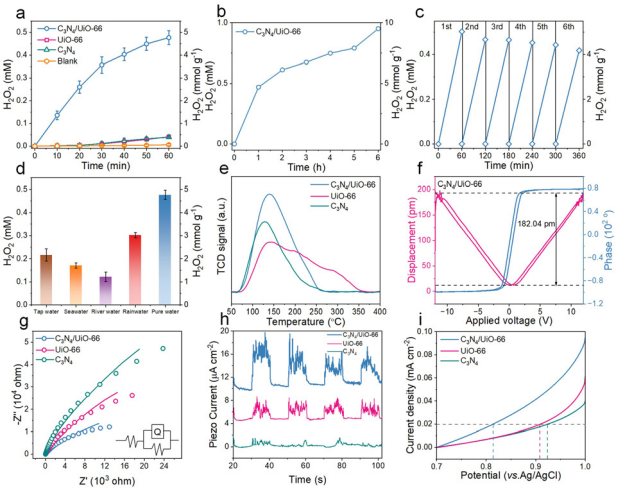

Fig. 2 (a) Curves for piezoelectric H_2O_2 production in the presence of, respectively, C_3N_4/UiO-66, UiO-66 and C_3N_4. Experimental conditions: catalyst (0.1 g L^{-1}) under ultrasound (Us), T = 25 °C. (b) Piezoelectric H_2O_2 production for 6 h. (c) and (d) H_2O_2 production in the presence of C_3N_4/UiO-66 (c) recycled every hour and (d) in different real water samples under Us. (e) Curves for O_2-TPD of C_3N_4/UiO-66, UiO-66 and C_3N_4. (f) Phase hysteresis loop and amplitude butterfly loop when using C_3N_4/UiO-66. (g) Nyquist plots with the fitted equivalent circuit based on EIS simulation. (h) Transient current density time curves over time under periodic Us signals and (i) LSV for C_3N_4/UiO-66, UiO-66 and C_3N_4.

from 25.97° in C_3N_4 to 27.3° in the composite, indicating a reduced interlayer spacing (Fig. 1a). A shifted (100) peak at 12° and the retained (111) peak of UiO-66 at 7.2° suggested strong interfacial interactions and maintained structural integrity.[26] Fourier-transform infrared spectroscopy (FT-IR) (Fig. 1b) showed characteristic peaks of triazine units at 810 cm^{-1} and 1200–1700 cm^{-1} for both C_3N_4 and the composite, with no evident COO^- signals, indicating a predominant C_3N_4 framework.[27] Zeta potential analysis (Fig. 1c) confirmed the occurrence of electrostatic attraction between negatively charged C_3N_4 (−21.8 mV) and positively charged UiO-66 (+ 31.7 mV), promoting a stable composite formation, and demonstrating their spontaneous electrostatic self-assembly.[14]

X-ray photoelectron spectroscopy (XPS) analysis further confirmed the formation of a strong electronic interface between C_3N_4 and UiO-66. Compare to the C 1s region of the spectrum (Fig. 1d and Fig. S4a and S5a), the composite yielded an intensified peak at 288.22 eV, attributed to C–N–Zr bonding, along with a shift in the C–N bond energy (286.49 eV), indicating interfacial charge redistribution. The N 1s region of the spectrum of the composite revealed an increased binding energy for N–H (400.31 eV) and decreased binding energy for C═N–C (398.68 eV) compared to those of pure C_3N_4, as shown in Fig. 1e and Fig. S4b and S5b, suggesting coordination between nitrogen atoms and Zr–O clusters.[28,29] These changes, together with the preserved pyrrole-N peak (401.35 eV), confirmed the structural integrity of the C_3N_4 framework and a modified electronic environment.[30] Compare to the Zr 3d region of the spectrum of the composite (Fig. 1f and Fig. S4c and S5c), a slight downshift in Zr $3d_{5/2}$ (182.78 eV) and upshift in Zr $3d_{3/2}$ (185.24 eV) were observed, and further indicated electronic interactions at the interface, leading to increased electron density around Zr sites.[31,32] These observations highlight the formation of a well-defined metal–semiconductor interface, which facilitates charge separation and enhances piezocatalytic activity.[33]

The piezocatalytic performance of the C_3N_4/UiO-66 composite showed a significant enhancement in H_2O_2 generation efficiency, demonstrating a production rate substantially surpassing those observed for the individual C_3N_4 and UiO-66 components under identical test conditions (Fig. 2a). As shown in Fig. 2b and c, the composite demonstrated remarkable stability, sustaining continuous operation over 6 h without significant activity loss and retaining over 90% of its initial performance after six cycles. Furthermore, the composite maintained good H_2O_2-generation capability in real water matrices such as tap water, seawater, river water, and rainwater, with only slight reductions in yield compared to pure water (Fig. 2d), primarily due to the presence of background organic and inorganic constituents that may have scavenged radicals or competed for active sites, highlighting its potential for practical applications. Mechanistic studies indicated the enhanced performance to be due to improved O_2 activation and interfacial charge dynamics. The obtained O_2 temperature-programmed desorption (O_2-TPD) results (Fig. 2e) revealed a significantly higher capacity of the composite than of the components to adsorb oxygen, while piezoresponse force microscopy (PFM) yielded a pronounced butterfly-shaped amplitude loop with a peak amplitude of 182.04 pm (Fig. 2f), confirming strong piezoelectric activity. Electrochemical impedance spectroscopy showed the composite having displayed the lowest charge-transfer resistance (Fig. 2g),[34] and piezoelectric current measurements indicated it to have the highest response (Fig. 2h) among all the samples.[35] Linear sweep voltammetry (LSV) further demonstrated a strong current response in the 0.7–1 V range (Fig. 2i). Consistent with these results, the open-circuit voltage (OCV) of C_3N_4/UiO-66 (0.347 V) was significantly higher than those of the individual components (0.112 and 0.166 V) (Fig. S6), confirming a stronger charge-separation driving force. To further evaluate the performances of the three materials, their IEF strengths were quantified using the Gouy–Chapman formula (Eqn. S1–S5).[36] The quantitative analysis demonstrated an IEF strength 1.17-times

higher for the C_3N_4/UiO-66 composite than for C_3N_4 (Fig. S7)—with the strong IEF enhancing charge separation, as further evidenced by the poor performance of physically mixed samples (Fig. S8). These findings collectively confirmed that interface engineering can significantly enhance charge separation and transport, enabling efficient piezocatalytic H_2O_2 generation.

Electron paramagnetic resonance (EPR) spectroscopy was employed to investigate the surface electronic states of the catalysts. As shown in Fig. 3a, all samples exhibited a Lorentzian signal centered at g = 2.003, corresponding to unpaired, non-localized electrons in the heptazine ring structure of C_3N_4.[37] Notably, the C_3N_4/UiO-66 composite showed a stronger signal intensity, which was not simply the sum of the individual contributions from C_3N_4 and UiO-66, indicating a higher content of localized unpaired electrons. This enhancement was attributed to interfacial ion-exchange interactions that promoted charge separation, thereby increasing the population of unpaired electrons and enhancing catalytic activity.

A predominantly ORR mechanism for the function of C_3N_4/UiO-66 was further supported the higher yield of H_2O_2 in the presence of O_2 and a significant decrease in H_2O_2 production in Ar (Fig. 3b).[38] To elucidate the reactive species involved, sacrificial agent experiments were conducted.[39] As shown in Fig. 3c, the addition of *p*-benzoquinone (*p*-BQ), a scavenger for superoxide radicals ($^*O_2^-$), led to a 94% decrease in H_2O_2 production, indicating $^*O_2^-$ to be the primary active species. The introduction of *tert*-butanol (TBA), a scavenger for hydroxyl radicals ($^\bullet$OH), resulted in a 36.1% decrease, suggesting $^\bullet$OH to be a secondary contributor. Furthermore, introduction of sodium iodate ($NaIO_3$), an electron scavenger, reduced the yield by 45.8%, whereas introducing the hole scavenger EDTA-2Na caused only a 7% reduction. These findings confirmed that H_2O_2 production proceeded predominantly *via* a $2e^-$ ORR pathway, with additional contributions from $2e^-$ and $4e^-$ WOR processes. EPR measurements using spin-trapping agents further validated the generation of $^*O_2^-$ and $^\bullet$OH radicals (Fig. 3d and e). The C_3N_4/UiO-66 composite exhibited stronger $^*O_2^-$ signals than did the individual components, highlighting its superior ability to activate O_2 and produce reactive intermediates. These results were found to be consistent with those from atmospheric control and quenching experiments, collectively confirming that the enhanced piezocatalytic H_2O_2 production arose from efficient interfacial charge separation and a predominant $^*O_2^-$-driven ORR pathway.[38,40]

Based on the previous discussions, a plausible piezoelectric catalytic mechanism for the C_3N_4/UiO-66 composites was derived, and is outlined in Fig. 4. The C_3N_4/UiO-66 composite material was concluded to generate H_2O_2 through a piezoelectric-field-driven dual pathway.[41] Under mechanical stress, such as ultrasound, the piezoelectric field generated by the piezoelectric material C_3N_4 interacts with the internal electric field at the interface, creating a coupled enhancement effect: the piezoelectric field drives the efficient separation of electron–hole pairs, with electrons (e^-) migrating directly to the Zr active sites of UiO-66 under the guidance of the IEF, generating H_2O_2 through the $2e^-$ ORR pathway; and holes (h^+) accumulate on the C_3N_4 surface under the dual electric field, producing $^\bullet$OH through the WOR pathway, with $^\bullet$OH then indirectly converted into H_2O_2 through radical coupling. This synergistic effect not only continuously provides a driving force through the piezoelectric field to overcome charge recombination but also precisely regulates the spatial distribution of e^-/h^+ *via* the IEF, enabling the ORR and WOR pathways to proceed efficiently in parallel, ultimately achieving a significant increase in H_2O_2 yield.

In summary, we successfully developed a C_3N_4/UiO-66 composite *via* electrostatic self-assembly, which exhibited a significantly enhanced IEF that promoted efficient piezocatalytic production of H_2O_2. The optimized composite achieved an outstanding H_2O_2-generation rate under ambient conditions, superior to those of C_3N_4 and UiO-66. The excellent performance was attributed to the strong IEF at the C_3N_4/UiO-66 interface, which promotes directional charge separation and facilitates carrier transport. Mechanistic studies revealed the engineered IEF not only facilitating effective charge separation

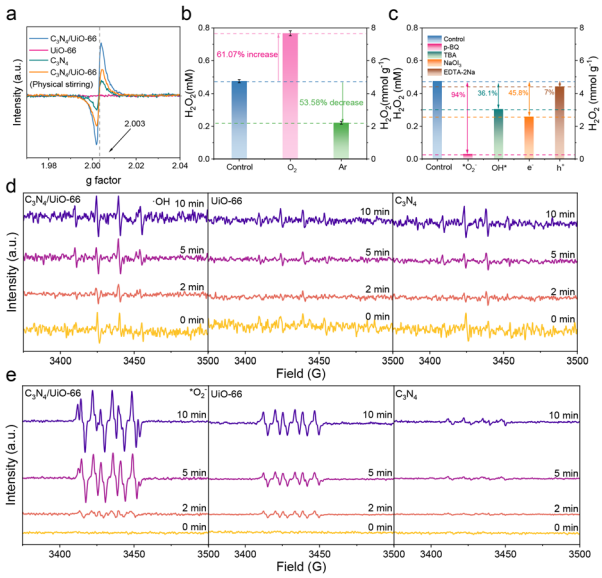

Fig. 3 (a) Plots of EPR intensity *versus* g-factor. (b) Piezoelectric H_2O_2 generation under different atmospheres. (c) Values of piezocatalytic H_2O_2 production at 60 min when including indicated scavengers (*p*-BQ for $^*O_2^-$, TBA for $^\bullet$OH, $NaOI_3$ for e^-, EDTA-2Na for h^+). (d) and (e) Plots of EPR intensity *versus* G for the detection of (d) DMPO–$^*O_2^-$ and (e) DMPO-$^\bullet$OH, each in the presence of C_3N_4/UiO-66, UiO-66 and C_3N_4, respectively.

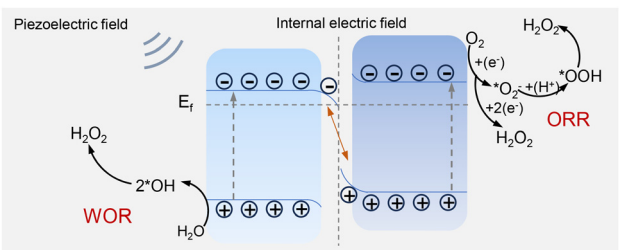

Fig. 4 Proposed reaction mechanism of H_2O_2 production piezocatalyzed by C_3N_4/UiO-66.

but also simultaneously promoting both ORR and WOR pathways, as evidenced by EPR detection of $^{*}O_2^{-}$ and $^{\bullet}OH$ radicals. This work presents a promising strategy for designing advanced piezocatalytic systems through interfacial engineering, paving the way for sustainable chemical synthesis using mechanical energy.

J. Y.: validation, investigation, writing – original draft. H. C.: formal analysis, methodology. J. L.: investigation, methodology. L.G.: writing – review & editing, supervision. Z. L.: conceptualization, writing – review & editing, supervision. M. Z.: resources, funding, writing – review & editing, supervision.

This work has been supported by the Science and Technology Program of Guangzhou (2024A04J6256). We are also grateful for the TEM and other technical support provided by Dr Xiang Yu of the Analytical and Testing Center of Jinan University.

Conflicts of interest

There are no conflicts to declare.

Data availability

The data supporting this article have been included as part of the supplementary information (SI). The experimental methods and characterisation data (TEM and XPS) supporting this article have been included in the SI. See DOI: **https://doi.org/10.1039/d5cc04517g**.

Notes and references

1 C. Xia, J. Y. Kim and H. Wang, *Nat. Catal.*, 2020, **3**, 605–607.
2 J. M. Campos-Martin, G. Blanco-Brieva and J. L. Fierro, *Angew. Chem., Int. Ed.*, 2006, **45**, 6962–6984.
3 R. J. Lewis and G. J. Hutchings, *ChemCatChem*, 2019, **11**, 298–308.
4 L. Zhao, M. Xu, S. Yang, Z. Zhu, J. Qi and F. Meng, *ACS Sustainable Chem. Eng.*, 2025, **13**, 8853–8869.
5 W. Qi, Y. Fu, E. Liu, Z. Cheng, Y. Sun, S. Liu and M. Yang, *EES Catal.*, 2024, **2**, 884–910.
6 Y. Chen, S. Lan and M. Zhu, *Chin. Chem. Lett.*, 2021, **32**, 2052–2056.
7 Z. Li, S. Lan and M. Zhu, *Environ. Sci. Ecotechnol.*, 2024, **18**, 100329.
8 Y. Zhang, Y. Lin, R. Li, Z. Chen, D. Zeng, S. Chen, W. Wang, L. Zhang, W. Wang and H. Nie, *Chem. Eng. J.*, 2023, **465**, 143043.
9 M. Zhang, W. Guo, Y. Chen, D. He, A. B. Isaev and M. Zhu, *Chin. Chem. Lett.*, 2023, **34**, 108229.
10 G. Li, Q. Zhong, W. Wu, Y. Liu, H. Li, X. Li and T. Long, *J. Colloid Interface Sci.*, 2025, **700**, 138431.
11 J. Yang, M. Zhang, M. Chen, Y. Zhou and M. Zhu, *Adv. Mater.*, 2023, **35**, 2209885.
12 J. Xu, H. Che, C. Tang, B. Liu and Y. Ao, *Adv. Mater.*, 2024, **36**, 2404539.
13 L. Chen, J. T. Ren and Z. Y. Yuan, *Adv. Energy Mater.*, 2023, **13**, 220372.
14 Y. Zhang, J. Qiu, B. Zhu, M. Fedin, B. Cheng, J. Yu and L. Zhang, *Chem. Eng. J.*, 2022, **444**, 136584.
15 K. Wang, Z. Shu, J. Zhou, Z. Zhao, Y. Wen and S. Sun, *J. Colloid Interface Sci.*, 2023, **648**, 242–250.
16 K. Wang, D. Shao, L. Zhang, Y. Zhou, H. Wang and W. Wang, *J. Mater. Chem. A*, 2019, **7**, 20383–20389.
17 D. Li, Q. Wen, C. Gao, Y. Zhang, H. Zhu, J. Dang, F. Song and J. Zhou, *Small*, 2025, **21**, 2500797.
18 H. Lv, Z. Li, P. Yin, P. Wan and M. Zhu, *Chin. Chem. Lett.*, 2025, **36**, 110457.
19 J. Chen, N. Kang, J. Fan, C. Lu and K. Lv, *Mater. Today Chem.*, 2022, **26**, 101028.
20 L. Tang, D. Zhou, Q. Chen and M. Zhu, *Surf. Interfaces*, 2025, **62**, 106269.
21 Z. Li, Y. Zhou, Y. Zhou, K. Wang, Y. Yun, S. Chen, W. Jiao, L. Chen, B. Zou and M. Zhu, *Nat. Commun.*, 2023, **14**, 5742.
22 Z. Yu, D. Wang, T. Zheng, A. Zavabeti, Y. Wang, C. Wu, J. Yang, Y. Guo, P. A. Webley and G. K. Li, *J. Mater. Chem. A*, 2025, **13**, 8368–8374.
23 Y. Wang, P. Su, Z. Lin, X. Li, K. Chen, T. Ye, Y. Li, Y. Zou and W. Wang, *Adv. Mater.*, 2025, **37**, 2418207.
24 J. He, Z. Yi, Q. Chen, Z. Li, J. Hu and M. Zhu, *Chem. Commun.*, 2022, **58**, 10723–10726.
25 Y. Li, Z. Li, X. Lin, H. Lv and M. Zhu, *Chem. Commun.*, 2023, **59**, 5749–5752.
26 W. Wang, S. Song, P. Wang, M. He, Z. Fang, X. Yuan, H. Li, C. Li, X. Wang and Y. Wei, *ACS Catal.*, 2023, **13**, 4597–4610.
27 X.-H. Yi, S.-Q. Ma, X.-D. Du, C. Zhao, H. Fu, P. Wang and C.-C. Wang, *Chem. Eng. J.*, 2019, **375**, 121944.
28 H. Wang, E. Almatrafi, Z. Wang, Y. Yang, T. Xiong, H. Yu, H. Qin, H. Yang, Y. He and C. Zhou, *J. Colloid Interface Sci.*, 2022, **608**, 1051–1063.
29 Y. Wang, L. Guo, Y. Zeng, H. Guo, S. Wan, M. Ou, S. Zhang and Q. Zhong, *ACS Appl. Mater. Interfaces*, 2019, **11**, 30673–30681.
30 R. Wang, L. Gu, J. Zhou, X. Liu, F. Teng, C. Li, Y. Shen and Y. Yuan, *Adv. Mater. Interfaces*, 2015, **2**, 1500037.
31 X. Zhang, Y. Yang, W. Huang, Y. Yang, Y. Wang, C. He, N. Liu, M. Wu and L. Tang, *Mater. Res. Bull.*, 2018, **99**, 349–358.
32 F. Yu, L. Chen, X. Shen, X. Li and C. Duan, *APL Mater.*, 2019, **7**, 101101.
33 X. Lu, Y. Shi, D. Tang, X. Lu, Z. Wang, N. Sakai, Y. Ebina, T. Taniguchi, R. Ma and T. Sasaki, *ACS Nano*, 2022, **16**, 4775–4785.
34 S. Wang, F. Chen, Z. Li, H. Tao, L. Qu, J. Li, M. Zhu and Q. Zha, *Surf. Interfaces*, 2023, **39**, 102910.
35 T. Jia, L. Wang, Z. Zhu, B. Zhu, Y. Zhou, G. Zhu, M. Zhu and H. Tao, *Chin. Chem. Lett.*, 2024, **35**, 108692.
36 J. Ke, J. Liu, H. Sun, H. Zhang, X. Duan, P. Liang, X. Li, M. O. Tade, S. Liu and S. Wang, *Appl. Catal., B*, 2017, **200**, 47–55.
37 Z. Li, H. Lv, K. Tong, Y. He, C. Zhai, Y. Yun and M. Zhu, *Appl. Catal., B*, 2024, **345**, 123690.
38 M. Song, W. Liu, J. Zhang, C. Zhang, X. Huang and D. Wang, *Adv. Funct. Mater.*, 2023, **33**, 2212087.
39 Y. Zhang, C. Pan, J. Li and Y. Zhu, *Acc. Mater. Res.*, 2023, **5**, 76–88.
40 C. Chen, K. Gu, P. Wang, Z. Q. Liu and Y. Ao, *Angew. Chem., Int. Ed.*, 2025, **64**, e202425656.
41 H. Chen, S. Gao, G. Huang, Q. Chen, Y. Gao and J. Bi, *Appl. Catal., B*, 2024, **343**, 123545.